ISSN 1674-1056
http://cpb.iphy.ac.cn
http://iopscience.iop.org/cpb
中国物理 B
Chinese Physics
中国物理 Chinese Physics B

Experimental demonstration of tight duality relation inthree-path interferometer

Zhi-Jin Ke(柯芝锦), Yu Meng(孟雨), Yi-Tao Wang(王轶韬), Shang Yu(俞上), Wei Liu(刘伟), Zhi-Peng Li(李志鹏), Hang Wang(汪航), Qiang Li(李强), Jin-Shi Xu(许金时), Jian-Shun Tang(唐建顺), Chuan-Feng Li(李传锋), Guang-Can Guo(郭光灿)

Citation: Chin. Phys. B . 2020, 29(5): 050307 . **doi:** 10.1088/1674-1056/ab7ea2
Journal homepage: http://cpb.iphy.ac.cn; http://iopscience.iop.org/cpb

What follows is a list of articles you may be interested in

Recast combination functions of coordinate and momentum operators into their ordered product forms

Lei Wang(王磊), Xiang-Guo Meng(孟祥国), Ji-Suo Wang(王继锁)
Chin. Phys. B . 2020, 29(5): 050303 . **doi:** 10.1088/1674-1056/ab7dbd

Optical complex integration-transform for deriving complex fractional squeezing operator

Ke Zhang(张科), Cheng-Yu Fan(范承玉), Hong-Yi Fan(范洪义)
Chin. Phys. B . 2020, 29(3): 030306 . **doi:** 10.1088/1674-1056/ab6dc9

Applicability of coupling strength estimation for linear chains of restricted access

He Feng(冯赫), Tian-Min Yan(阎天民), Yuhai Jiang(江玉海)
Chin. Phys. B . 2020, 29(3): 030305 . **doi:** 10.1088/1674-1056/ab6c43

Quantifying non-classical correlations under thermal effects in a double cavity optomechanical system

Mohamed Amazioug, Larbi Jebli, Mostafa Nassik, Nabil Habiballah
Chin. Phys. B . 2020, 29(2): 020304 . **doi:** 10.1088/1674-1056/ab65b6

Optimal phase estimation with photon-number difference measurement using twin-Fock states of light

J H Xu(徐佳慧), J Z Wang(王建中), A X Chen(陈爱喜), Y Li(李勇), G R Jin(金光日)
Chin. Phys. B . 2019, 28(12): 120303 . **doi:** 10.1088/1674-1056/ab4e7f

---

Experimental demonstration of tight duality relation in three-path interferometer*

Zhi-Jin Ke(柯芝锦)[1,2], Yu Meng(孟雨)[1,2], Yi-Tao Wang(王轶韬)[1,2], Shang Yu(俞上)[1,2], Wei Liu(刘伟)[1,2], Zhi-Peng Li(李志鹏)[1,2], Hang Wang(汪航)[1,2], Qiang Li(李强)[1,2], Jin-Shi Xu(许金时)[1,2], Jian-Shun Tang(唐建顺)[1,2,†], Chuan-Feng Li(李传锋)[1,2,‡], and Guang-Can Guo(郭光灿)[1,2]

[1] *CAS Key Laboratory of Quantum Information, University of Science and Technology of China, Hefei* 230026, *China*

[2] *CAS Center For Excellence in Quantum Information and Quantum Physics, University of Science and Technology of China, Hefei* 230026, *China*

(Received 22 February 2020; revised manuscript received 4 March 2020; accepted manuscript online 11 March 2020)

Bohr's principle of complementarity has a long history and it is an important topic in quantum theory, among which the famous example is the duality relation. The relation between visibility C and distinguishability D, $C^2+D^2\leq 1$, has long been recognized as the only representative of the duality relation. However, recent researches have shown that this inequality is not good enough because it is not tight for multipath interferometers. Meanwhile, a tight bound for the multipath interferometer has been put forward. Here we design and experimentally implement a three-path interferometer coupling with path indicator states. The wave property of photons is characterized by l_1-norm coherence measure, and the particle property is based on distinguishability of the indicator states. The new duality relation of the three-path interferometer is demonstrated in our experiment, which bounds the union of a right triangle and a part of elliptical area inside the quadrant of a unit circle. Data analysis confirms that the new bound is tight for photons in three-path interferometers.

Keywords: duality relation, multi-path interferometer, principle of complementarity, foundations of quantum mechanics

PACS: 03.65.–w, 42.50.Xa, 03.65.Ta, 42.50.Ex **DOI:** 10.1088/1674-1056/ab7ea2

1. Introduction

Wave–particle duality is the well-known example of Bohr's complementarity principle.[1,2] The principle claims that, a particle that goes through an interferometer can exhibit either wave or particle properties. If one has the complete knowledge that which path the particle takes, then it is impossible to have any knowledge about the wave property, vice versa. In general, the duality relation indicates that, an increase knowledge of one property will result in a decrease in the other, which has been studied experimentally.[3–6] In 1978, Wooters and Zurek firstly investigated this intermediate case in theory.[7] In 1988, Greenberger and Yasin put forward an inequality to express the trade off relation between these two properties[8]

$$C^2+D^2\leq 1, \tag{1}$$

where C is the visibility of the interference pattern and D is a measure of the path information, i.e., the path distinguishability or the which-path information. In 1996, Englert introduced the "detectors" into the paths, whose status changes if a particle passes through them, and he used the distinguishability of the status of the detectors as a measure of the path information,[9] as shown in Fig. 2. To avoid ambiguity, we will call Englert's detector states as indicator states in our work, because they only indicate which path a photon takes, and never detect or destroy the photon. The inequality given in Eq. (1) has been experimentally verified by various quantum systems, such as nuclear magnetic resonance (NMR),[10,11] cold neutral atoms,[12,13] superconducting quantum circuits,[14] and single photons in delayed-choice scheme.[15–18] In 2014, the theory of quantum coherence as a resource was proposed along with an l_1-norm coherence measure.[19,20] Researchers found that the coherence measure is a natural candidate to quantify the wave-like property. Bera *et al.*[21] firstly used the l_1-norm coherence for wave property. Then Bagan *et al.* stepped further. They derived the duality relation for the multipath interferometer, which made use of the l_1-norm coherence measure and the probability of successfully distinguishing the indicator states by using minimum-error discrimination.[22] Soon after, the result was demonstrated by Yuan *et al.*[23] Finally, in 2018, they put forward the tightest form of the duality relation

*Project supported by the National Key Research and Development Program of China (Grant Nos. 2016YFA0302700 and 2017YFA0304100), the National Natural Science Foundation of China (Grant Nos. 11822408, 11674304, 11774335, 61490711, 11474267, 11821404, 11325419, 11904356, and 91321313), the Youth Innovation Promotion Association, Chinese Academy of Sciences (Grant No. 2017492), the Foundation for Scientific Instrument and Equipment Development, Chinese Academy of Sciences (Grant No. YJKYYQ20170032), the Key Research Program of Frontier Sciences, Chinese Academy of Sciences (Grant No. QYZDY-SSW-SLH003), the Fundamental Research Funds for the Central Universities, China (Grant Nos. WK2470000026 and WK2030000008), Science Foundation of Chinese Academy of Sciences (Grant No. ZDRW-XH-2019-1), Anhui Initiative in Quantum Information Technologies, China (Grant Nos. AHY020100, AHYPT003, and AHY060300), the National Postdoctoral Program for Innovative Talents of China (Grant No. BX20180293), and the China Postdoctoral Science Foundation (Grant No. 2018M640587).

†Corresponding author. E-mail: tjs@ustc.edu.cn

‡Corresponding author. E-mail: cfli@ustc.edu.cn

© 2020 Chinese Physical Society and IOP Publishing Ltd

in multipath interferometer.[24] Here is the tightest form

$$\left(\frac{C+D-\frac{n-2}{n-1}}{\frac{\sqrt{n}}{n-1}}\right)^2+\left(\frac{C-D}{\sqrt{\frac{n}{n-1}}}\right)^2\leq 1, \tag{2}$$

where n represents the number of paths of an interferometer. When $n=2$, i.e., for two-path interferometers, the inequality will degrade to Eq. (1). Once $n>2$, it bounds the area that contains a part of an elliptical area and a right triangle area in the first quadrant, as can be seen in Fig. 1. The center O of the elliptical area is located at $C=D=\frac{n-2}{2(n-1)}$, and its semimajor axis is parallel to line $C+D=1$. Until now, this new duality relation has not yet been verified in experiments.

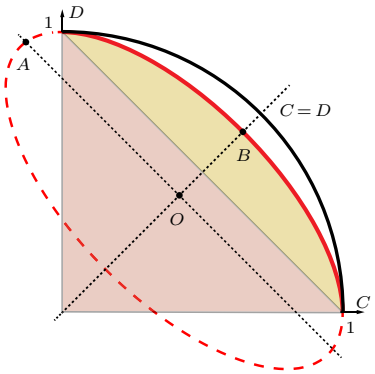


Fig. 1. Theoretical diagram of the tight new duality relation in multipath interferometers. C and D are the horizontal and vertical coordinates, respectively. The black line is a quarter of a unit cycle, which is described by Eq. (1) and used as a reference. The red line is a part of an ellipse, whose center O and seminor axis OB lie on the line $C=D$, and semimajor axis OA is parallel to the line $C+D=1$. This ellipse is described by Eq. (2) when $n=6$. The union of yellow and pink regions reveals the area that the tight duality relation bounds in a six-path interferometer.

In this paper, we experimentally demonstrate this new duality relation based on the coherence measure. With the help of a three-path Mach–Zehnder interferometer, we can fill in the experimental gap in this fields. The states of photons are encoded on the path basis, while the indicator states are encoded on the height degree of freedom, which is well-designed to simplify the experiment. The wave property of the photons is characterized by the l_1-norm coherence measure and the particle property of the photons is characterized by the distinguishability of the indicator states. We use quantum states with different coherence as the input states. The states with maximal coherence lie on the bound that equation (2) describes. As for the states with non-maximal coherence, they locate inside the bound. Based on the experimental data, we can plot out the tight bound that the new theory predicts. Comparing with the line describe by Eq. (1), this new bound has a more accurate description about the multi-path interferometers.

2. Duality relation in three-path interferometer

Figure 2 is the schematic representation of a three-path interferometer in our experiment. Let $n=3$ in Eq. (2), we can achieve

$$\left(\frac{C+D-\frac{1}{2}}{\sqrt{3}/2}\right)^2+\left(\frac{C-D}{\sqrt{3}/2}\right)^2\leq 1, \tag{3}$$

where C represents the visibility and D represents the distinguishablity. A photon that enters a three-path interferometer will be in a superposition state $|\psi\rangle=(x_0|0\rangle+x_1|1\rangle+x_2|2\rangle)$, where x_i $(i\in\{0,1,2\})$ are the coefficients and the orthogonal basis states $|0\rangle$, $|1\rangle$, and $|2\rangle$ correspond to path 0, path 1, and path 2 in the interferometer, respectively. Path indicators are introduced into each path to obtain the path information of the photons. At first, the path indicators are all in the same initial state $|i\rangle$, then if a photon passes through path 0, the indicator in path 0 will end in state $|\eta_0\rangle$. The other two possible statuses of the path indicators are $|\eta_1\rangle$ and $|\eta_2\rangle$, corresponding to the other two paths, respectively. Thus, if the indicator is found to be, e.g., $|\eta_1\rangle$, the photon is considered to travel through path 1, which is based on the minimum-error discrimination method.[9] Note that, the photons interact with the path indicator system, so they can be expressed as $|\Psi\rangle=(x_0|0\rangle|\eta_0\rangle+x_1|1\rangle|\eta_1\rangle+x_2|2\rangle|\eta_2\rangle)$. Here,

$$\begin{aligned}
|\eta_0\rangle &= \sin\theta|\alpha\rangle+\frac{\sqrt{2}}{2}\cos\theta|\beta\rangle+\frac{\sqrt{2}}{2}\cos\theta|\gamma\rangle,\\
|\eta_1\rangle &= \frac{\sqrt{2}}{2}\cos\theta|\alpha\rangle+\sin\theta|\beta\rangle+\frac{\sqrt{2}}{2}\cos\theta|\gamma\rangle,\\
|\eta_2\rangle &= \frac{\sqrt{2}}{2}\cos\theta|\alpha\rangle+\frac{\sqrt{2}}{2}\cos\theta|\beta\rangle+\sin\theta|\gamma\rangle,
\end{aligned} \tag{4}$$

where $|\alpha\rangle$, $|\beta\rangle$, and $|\gamma\rangle$ are three orthogonal bases of another degree of freedom in the vertical directions (height) of the original photon paths, and $\theta\in(35.3^\circ,90.0^\circ]$.

The critical feature of the indicator states is that, the overlap of any two of them is a constant when θ is fixed, which is one of the two necessary conditions for a state to reach the bound in Eq. (2). The other one is that the state must has maximal coherence.

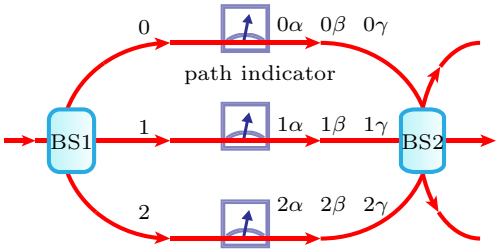


Fig. 2. Schematic representation of a three-path interferometer with path indicators. The status of the path indicators changes when a photon passes through them. BS1 is short for a three-port beam splitter and BS2 is a nine-port beam splitter. The light paths are labeled as 0, 1, 2 after BS1, and the nine light paths are labeled as path ab ($a\in\{0,1,2\}$ and $b\in\{\alpha,\beta,\gamma\}$) after the path indicators. The degree of freedom $\{\alpha,\beta,\gamma\}$ will be traced out when we collect the experimental data, therefore only three paths are displayed after the path indicators.

The $|\Psi\rangle$ describes the entanglement between the photons and the indicator system, however, the duality relation is the property of photons. Thus, we should trace out the indicator

system first to obtain the density matrix of the photons, which is

$$\rho = \mathrm{Tr}_{\mathrm{indicator}}(|\Psi\rangle\langle\Psi|) = \sum_{i,j=0}^{2} x_i x_j^* \langle\eta_j|\eta_i\rangle |i\rangle\langle j|. \quad (5)$$

Then, the l_1-norm coherence of the photons is calculated[19] by

$$C_{l_1}(\rho) = \sum_{i,j=0, i\neq j}^{2} |\rho_{ij}|. \quad (6)$$

Finally, we obtain the formula to calculate visibility C in Eq. (3), that is

$$C = \frac{1}{2} C_{l_1}(\rho) \quad (7)$$

given in Ref. [24].

The path information D of the photons is calculated based on the discrimination ability of indicator states $\{|\eta_i\rangle\}$. For N non-orthogonal quantum states $\{|\eta_i\rangle\}$, the discrimination ability is the average probability of successfully identifying the states, that is

$$P_{\mathrm{d}} = \sum_{i=0}^{N-1} p_i \langle\eta_i|\Pi_i|\eta_i\rangle, \quad (8)$$

where p_i is the occurring probability of state $|\eta_i\rangle$, and $\{\Pi_i\}$ are N positive operator-valued measures (POVMs) corresponding to $\{|\eta_i\rangle\}$. Once P_{d} is evaluated, we obtain the following formula of D for the three-path interferometer in Eq. (3) according to Refs. [24,25]:

$$D = \frac{3}{2}\left(P_{\mathrm{d}} - \frac{1}{3}\right). \quad (9)$$

3. Experimental setup

The entire experimental setup is shown in Fig. 3. There are two modules, a) state preparation and indicator state encoding module and b) measurement module. The single photon source is generated by the type-II spontaneous parametric down-conversion (SPDC), with the counting rate about 10000 counts per second. The central wavelength is 440 nm.

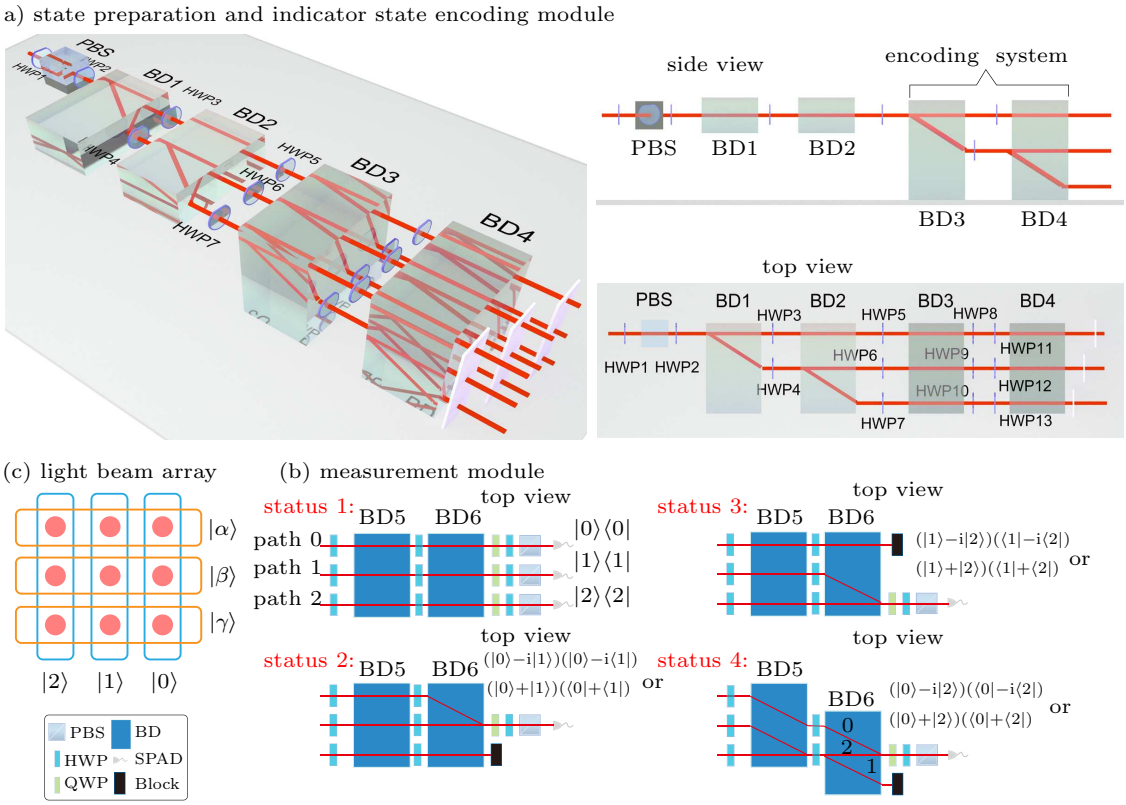


Fig. 3. Experimental setup. There are two parts of the setup, (a) state preparation and indicator state encoding module (with a 3D view, a side view, and a top view) and (b) measurement module with its four statuses in top view. (c) Light beam array, the view comes from a person who faces the light source at the end of (a). The nine paths will then enter the measurement module. The paths have two coordinates, the horizontal one tells which interferometer arm a path belongs to, and the vertical one tells the layer information of a path. Each indicator state is labeled with a pink rectangle box in (a) and with a blue rectangle box in (c). Measurement bases labeled in (b) are used to perform tomography of each layer of the light beam array in (c). BD1 and BD2 are the correspondence of the first BS in Fig. 2, and BD5 and BD6 in measurement module can be seen as the correspondence of the second BS, which has nine light paths.

In the state preparation module, the input state is in horizontal polarization (or H-polarization) after the polarization beam splitter (PBS), denoted as $|\mathrm{H}\rangle$. Similarly, the vertical polarization (V-polarization) is denoted as $|\mathrm{V}\rangle$. After passing the half-wave plate 2 (HWP2) with a certain rotation angle ϕ, the state of $(\cos\phi|\mathrm{H}\rangle + \sin\phi|\mathrm{V}\rangle)$ is generated. The beam displacer 1 (BD1) then causes the V-polarization component to be transmitted directly and the H-polarization component to

undergo a 4-mm lateral displacement. The H-polarization will continue to go through HWP4 with rotation angle ψ. At the output port of BD2, the state is $\sin\phi|0\rangle_{\rm V}+\cos\phi\sin\psi|1\rangle_{\rm V}+\cos\phi\cos\psi|2\rangle_{\rm H}$. Choosing suitable angle pairs (ϕ,ψ), we can prepare both maximal and non-maximal coherent states. Note that, the state is encoded on the path degree of freedom, and the polarization degree of freedom is just used to manipulate the path of the photons. For example, let the photon in H-polarization, then it will travel to next path after passing a BD.

In the indicator state encoding module (BD3 and BD4), the optical axes lie in the vertical plane, thus in turn the V-polarization component will undergo a 4-mm vertical displacement after passing a BD. The rotation angles of the HWPs (from 5 to 13) in this module decide the θ in the indicator states in Eq. (4). Figure 3(c) shows the light beam array at the end of this module. There will be nine light paths, because there are originally three paths (arranged in the horizontal direction, see the top view), then each path has another three paths in the indicator system (arranged in the vertical direction, see the side view), which then give a 3 by 3 light beam array.

The measurement module is mainly consisted of another two BDs (BD5 and BD6, only shown in the top view), nine sets of QWP–HWP–PBS combinations (QWP stands for quarter wave plate), and nine single-photon avalanche diodes (SPADs). BD5 and BD6 combine any two horizontal paths in the same row (orange box) in the light beam array shown in Fig. 3(c). The measurement of each row is independent of the others. The QWP–HWP–PBS combinations provide measurement on polarization bases $|{\rm H}\rangle$, $|{\rm V}\rangle$, $|{\rm H}\rangle+|{\rm V}\rangle$, and $|{\rm H}\rangle-{\rm i}|{\rm V}\rangle$. Finally, the photons are collected into fibers and detected by nine SPADs.

4. Evaluation of visibility and distinguishablity

Visibility C and distinguishablity D are calculated based on photon counts from the SPADs. The photon counts of each path in light beam array in Fig. 3(c) can be described as n_{ab} ($a\in\{\alpha,\beta,\gamma\}$ and $b\in\{0,1,2\}$).

The density matrix of photons in the three-path interferometer is a 3 by 3 matrix. Given that the nine paths in our experimental setup can be divided into three parts (see the three orange rectangle boxes in Fig. 3(c)), so one feasible way to reconstruct the density matrix ρ is to reconstruct each part $(\rho_\alpha,\rho_\beta,\rho_\gamma)$, respectively. Then combine them together as $\rho=(p_\alpha\rho_\alpha+p_\beta\rho_\beta+p_\gamma\rho_\gamma)$ (p_α, p_β, and p_γ are the normalization coefficients, see Appendix A for their values and the derivation of ρ).

Firstly, we reconstruct ρ_α, that is to evaluate the nine elements in the following matrix:

$$\begin{pmatrix}\rho_{00}&\rho_{01}&\rho_{02}\\ \rho_{10}&\rho_{11}&\rho_{12}\\ \rho_{20}&\rho_{21}&\rho_{22}\end{pmatrix}_\alpha. \tag{10}$$

The diagonal elements represent the proportion of photon counts in α basis of the three paths (first row in Fig. 3(c)), which can be directly acquired from the photon counts in each path in unit time. According to the analysis, we can directly obtain

$$\begin{aligned}&n_{\alpha,\rm tot}=n_{\alpha0}+n_{\alpha1}+n_{\alpha2},\\ &\rho_{00}=\frac{n_{\alpha0}}{n_{\alpha,\rm tot}},\quad \rho_{11}=\frac{n_{\alpha1}}{n_{\alpha,\rm tot}},\quad \rho_{22}=\frac{n_{\alpha2}}{n_{\alpha,\rm tot}}.\end{aligned} \tag{11}$$

As for the other six elements in Eq. (10), they are generally complex numbers, thus we should both evaluate the real and imaginary parts. Here we take the evaluation of ρ_{01} as an example,

$$\begin{aligned}{\rm Re}(\rho_{01})&=\frac{n_{|0\rangle+|1\rangle}-\frac{1}{2}(n_{|0\rangle}+n_{|1\rangle})}{n_{\alpha,\rm tot}},\\ {\rm Im}(\rho_{01})&=\frac{n_{|0\rangle-i|1\rangle}-\frac{1}{2}(n_{|0\rangle}+n_{|1\rangle})}{n_{\alpha,\rm tot}},\end{aligned} \tag{12}$$

where $n_{\rm basis}$ represents the photon counts under a specific measurement basis. The formulas are similar for the other elements in Eq. (10).

Unfortunately, it is impossible to directly measure on the superposition bases in the path basis, i.e., $|0\rangle+|1\rangle$ and $|0\rangle-{\rm i}|1\rangle$. Therefore, we transform the path basis into the polarization basis. That is, let photons in path 0 have H-polarization and photons in path 1 have V-polarization, combine two paths as shown in status 2 in Fig. 3(b), then basis $|0\rangle+|1\rangle$ will be transformed into $|{\rm H}\rangle+|{\rm V}\rangle$, and $|0\rangle-{\rm i}|1\rangle$ into $|{\rm H}\rangle-{\rm i}|{\rm V}\rangle$. According to these settings, we can evaluate ρ_{01} by Eq. (12). Following a similar process, all elements in Eq. (10) can be evaluated.

Then, we can evaluate ρ_β and ρ_γ with the same method. Once the density matrix ρ is acquired, C is calculated according to Eq. (7).

Now we turn to the evaluation of D. It is calculated according to the minimum-error state discrimination. In our experiment, there are three indicator states with their corresponding POVMs $\Pi_0=|\alpha\rangle\langle\alpha|$, $\Pi_1=|\beta\rangle\langle\beta|$, and $\Pi_2=|\gamma\rangle\langle\gamma|$. Then, each term in Eq. (8) is equal to each other, which is $\langle\eta_i|\Pi_i|\eta_i\rangle=\sin^2\theta$ ($i\in\{0,1,2\}$). Note that, $\sin\theta$ is larger than $\frac{\sqrt{2}}{2}\cos\theta$ for $\theta\in(35.3^\circ,90.0^\circ]$ in indicator states. Therefore, this POVM actually gets the proportion of the maximum output among three bases (α,β,γ) in an indicator state. Each term of $P_{\rm d}$ is calculated by

$$\begin{aligned}&n_{i,\rm tot}=n_{\alpha i}+n_{\beta i}+n_{\gamma i},\quad i\in\{0,1,2\},\\ &P_{\rm s0}=\frac{n_{\alpha0}}{n_{0,\rm tot}},\quad P_{\rm s1}=\frac{n_{\beta1}}{n_{1,\rm tot}},\quad P_{\rm s2}=\frac{n_{\gamma2}}{n_{2,\rm tot}}.\end{aligned} \tag{13}$$

In our experimental setup, the photons have probability $|x_i|^2$ to enter the i-th path of the interferometer, thus $p_i=|x_i|^2$ ($i\in\{0,1,2\}$) in Eq. (8). Finally, D is calculated using Eq. (9).

5. Analysis of data

As analysis shown in Ref. [26], loss of photons inside and outside the interferometers affects the results of duality relation in an interferometer. There are several possible systematic errors in our setup. They possibly come from the state preparation, indicator state encoding, difference in fiber coupling efficiency, or difference in SPAD detection efficiency. Therefore, we have calibration for our experimental setup before data collection. Firstly, we let the coupling efficiency of all fibers between 60% to 62%. Given that the photon counts of the nine light paths in Fig. 3(c) have accurate ratio once the input states and θ in the indicators states are determined. Thus, we make sure that the ratio of photon counts from the SPADs is around the correct ratio by adjusting the angles of the HWPs (HWP2 to HWP13). We cannot achieve a ratio exactly equal to the theory because of statistical errors. This method compensates the systematic errors both inside and outside the interferometer.

Based on the measurement described above, we can obtain the C and D of various input states for different θ of the indicator states. We use three different input states as demonstration, one is the maximal coherent state, and the other two are states with lower coherence.

In Fig. 4, the circle points are the experimental results of maximal coherent state $\frac{1}{\sqrt{3}}(|0\rangle+|1\rangle+|2\rangle)$ with θ from 35.3° to 90.0°. ΔC (ΔD) is the standard deviation of C (D), represented by the blue horizontal (red vertical) error bars. Since we have calibrated our setups, the errors are dominated by statistical errors.

When $\theta = 35.3°$, the data point ① lies on $(0.9956 \pm 0.0134,\ 0.0028 \pm 0.0048)$, because now the three indicator states in Eq. (4) are the same as each other. In other words, they are indistinguishable, thus the photons have the minimum in their particle property and achieve the maximum in their wave property. With the angle increasing, the indicator states become more and more distinguishable, thus the particle property of the photons (D) increases while the wave property (C) decreases. When $\theta = 90.0°$, the three indicator states are orthogonal to each other, thus we can discriminate them and determine which path the photons take with certainty. Therefore, the data point ⑦ lies on $(0.0103 \pm 0.0063,\ 0.9938 \pm 0.0006)$, where only particle property exists. The relation between C and D here satisfies the definition of duality relation, because the increase of one causes the decrease of the other, and vice versa.

The triangle points are the experimental results of state $0.78|0\rangle + 0.38|1\rangle + 0.50|2\rangle$. The rhombus points are the results of state $0.88|0\rangle + 0.28|1\rangle + 0.38|2\rangle$. They are both non-maximal coherent states, but the states represented by triangle have much coherence than those by rhombus based on l_1-norm coherence measure. According to the location of these three kinds of points, we can infer that, the less coherence in a state, the closer the points will get to the origin.

Here is the analysis of why the bound provided by Eq. (3) is tight. The orange solid line in Fig. 4 is the theoretical bound of duality relation for a three-path interferometer provided by Eq. (3). The experimental points of maximal coherent state ① to ⑦ all lie on this bound. Given that, we could not find states with more coherence than the maximal coherent state, therefore, the states can only lie on the bound or inside the bound. The black dash line is the quadrant of a unit circle, described by Eq. (1). The space between these two lines are unreachable, thus the bound provided by Eq. (1) is not tight based on the experimental results from our setup.

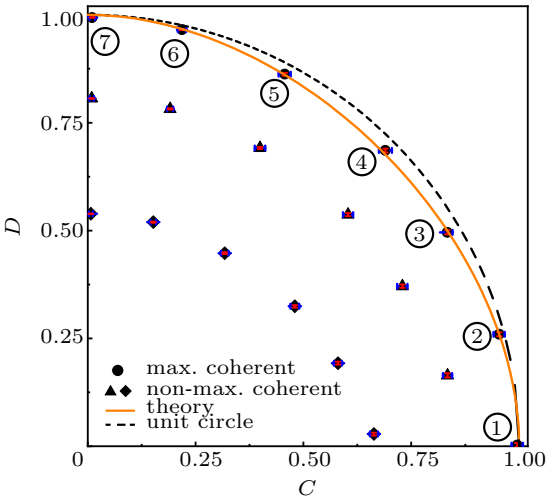


Fig. 4. Experiment data. The orange solid line is the theoretical tight bound of duality relation in a three-path interferometer, described by Eq. (3). The circle points are the experimental results of the state with maximal coherence. They lie on the theoretical bound and they move along the bound when θ in the indicator states $\{|\eta_i\rangle\}$ varies. While the triangle and rhombus points are the experimental results of two other states without maximal coherence. The states represented by triangle have much coherence than those represented by rhombus. We use l_1-norm coherence measure to quantify all these states. The black dash line is the quadrant described by Eq. (1), and it is used as a reference.

6. Conclusion

We have reported the results of the first experiment to demonstrate the duality relation of a three-path interferometer. The duality relation demonstrated here is tight because only states with maximal coherence are able to reach the bound as the theory predicts. While the states with lower coherence locate inside the bound. In our experiment, we encoded the input state onto path basis and the indicator states onto height basis, which significantly simplifies our experiment. With the well-designed setup, it is convenient for us to achieve the good interference visibility of any two paths on the same row of the light beam array. Due to the high precision of our experiment, we found good agreement with the theoretical predictions. Because the new bound demonstrated here is tight, it is possible to design a new method to detect a state with maximal coher-

ence in a multi-path interferometer according to the duality relation.

Appendix A: Derivation of ρ in three-path interferometer

After a photon going through the indicator encoding system, it has nine possible output ports shown in Fig. 3(c) in the main text. The wave function of the composite system is

$$|\Psi\rangle = (x_0|0\rangle|\eta_0\rangle + x_1|1\rangle|\eta_1\rangle + x_2|2\rangle|\eta_2\rangle). \tag{A1}$$

Then, the density matrix of the entire system is

$$\rho_{\rm sys} = |\Psi\rangle\langle\Psi| = \sum_{i,j=0}^{2} x_i x_j^* |i\rangle|\eta_i\rangle\langle j|\langle\eta_j|. \tag{A2}$$

Tracing out the indicator system, we obtain the density matrix ρ of the photon

$$\rho = \sum_{i,j=0}^{2} x_i x_j^* \langle\eta_j|\eta_i\rangle |i\rangle\langle j|. \tag{A3}$$

Note that, the three indicator states are non-orthogonal to each other, which are

$$\begin{aligned}
|\eta_0\rangle =& \sin\theta|\alpha\rangle + \frac{\sqrt{2}}{2}\cos\theta|\beta\rangle + \frac{\sqrt{2}}{2}\cos\theta|\gamma\rangle,\\
|\eta_1\rangle =& \frac{\sqrt{2}}{2}\cos\theta|\alpha\rangle + \sin\theta|\beta\rangle + \frac{\sqrt{2}}{2}\cos\theta|\gamma\rangle,\\
|\eta_2\rangle =& \frac{\sqrt{2}}{2}\cos\theta|\alpha\rangle + \frac{\sqrt{2}}{2}\cos\theta|\beta\rangle + \sin\theta|\gamma\rangle,
\end{aligned} \tag{A4}$$

where $|\alpha\rangle, |\beta\rangle, |\gamma\rangle$ are a set of orthogonal basis. Thus, we can obtain

$$\begin{aligned}
&\langle\eta_1|\eta_0\rangle = \langle\eta_0|\eta_1\rangle\\
=&\frac{\sqrt{2}}{2}\cos\theta\sin\theta\langle\alpha|\alpha\rangle + \frac{\sqrt{2}}{2}\cos\theta\sin\theta\langle\beta|\beta\rangle\\
&+ \frac{1}{2}\cos^2\theta\langle\gamma|\gamma\rangle.
\end{aligned} \tag{A5}$$

The other seven elements of ρ have the similar structure.

From Eq. (A5) we can know, each element consists of three parts, which come from the height degree of freedom $\{\alpha,\beta,\gamma\}$, and these three parts correspond to three layers (rows) of the light beam array shown in Fig. 3(c).

Based on these three parts, the density matrix can be reorganized as

$$\rho = (p_\alpha\rho_{\langle\alpha|\alpha\rangle} + p_\beta\rho_{\langle\beta|\beta\rangle} + p_\gamma\rho_{\langle\gamma|\gamma\rangle}), \tag{A6}$$

where $\rho_{\langle\alpha|\alpha\rangle}$ consists of all coefficients of $\langle\alpha|\alpha\rangle$ divided by p_α in $\{\langle\eta_i|\eta_j\rangle\}$ $(0\le i,j\le 2)$. $\rho_{\langle\beta|\beta\rangle}$ and $\rho_{\langle\gamma|\gamma\rangle}$ have the similar structure. p_α, p_β, and p_γ are the normalization coefficients. They are

$$\begin{aligned}
p_\alpha =& |x_0|^2\sin^2\theta + |x_1|^2\frac{1}{2}\cos^2\theta + |x_2|^2\frac{1}{2}\cos^2\theta,\\
p_\beta =& |x_0|^2\frac{1}{2}\cos^2\theta + |x_1|^2\sin^2\theta + |x_2|^2\frac{1}{2}\cos^2\theta,\\
p_\gamma =& |x_0|^2\frac{1}{2}\cos^2\theta + |x_1|^2\frac{1}{2}\cos^2\theta + |x_2|^2\sin^2\theta.
\end{aligned} \tag{A7}$$

Finally, we obtain the density matrix for the experimental implementation in the main text

$$\rho = (p_\alpha\rho_\alpha + p_\beta\rho_\beta + p_\gamma\rho_\gamma), \tag{A8}$$

where α,β,γ are short for $\langle\alpha|\alpha\rangle, \langle\beta|\beta\rangle, \langle\gamma|\gamma\rangle$.

Therefore, each layer contains the partial but independent information of the entire system, which corresponds to ρ_α, ρ_β, and ρ_γ. In our experiment, we do tomography for each layer and finally add them together to acquire the density matrix ρ.

References

[1] Bohr N 1928 *Nature* **121** 580
[2] Bohr N 1928 *Naturwissenschaften* **16** 245
[3] Rauch H and Summhammer J 1984 *Phys. Lett. A* **104** 44
[4] Summhammer J, Rauch H and Tuppinger D 1987 *Phys. Rev. A* **36** 4447
[5] Buks E, Schuster R, Heiblum M, Mahalu D and Umansky V 1998 *Nature* **391** 871
[6] Dürr S, Nonn T and Rempe G 1998 *Nature* **395** 33
[7] Wootters W K and Zurek W H 1979 *Phys. Rev. D* **19** 473
[8] Greenberger D M and Yasin A 1988 *Phys. Lett. A* **128** 391
[9] Englert B G 1996 *Phys. Rev. Lett.* **77** 2154
[10] Peng X H, Zhu X W, Fang X M, Feng M, Liu M L and Gao K L 2003 *J. Phys. A: Math. Gen.* **36** 2555
[11] Peng X H, Zhu X W, Suter D, Du J F, Liu M L and Gao K L 2005 *Phys. Rev. A* **72** 052109
[12] Dürr S, Nonn T and Rempe G 1998 *Phys. Rev. Lett.* **81** 5705
[13] Wang Z H, Tian Y L, Yang C, Zhang P F, Li G and Zhang T C 2016 *Phys. Rev. A* **94** 062124
[14] Zheng S B, Zhong Y P, Xu K, Wang Q J, Wang H, Shen L T, Yang C P, Martinis, J M, Cleland A N and Han S Y 2015 *Phys. Rev. Lett.* **115** 260403
[15] Kaiser F, Coudreau T, Milman P, Ostrowsky D B and Tanzilli S 2012 *Science* **338** 637
[16] Peruzzo A, Shadbolt P, Brunner N, Popescu S and O'Brien J L 2012 *Science* **338** 634
[17] Tang J S, Li Y L, Xu X Y, Xiang G Y, Li C F and Guo G C 2012 *Nat. Photon.* **6** 600
[18] Ma X S, Kofler J and Zeilinger A 2016 *Rev. Mod. Phys.* **88** 015005
[19] Baumgratz T, Cramer M and Plenio M B 2014 *Phys. Rev. Lett.* **113** 140401
[20] Streltsov A, Adesso G and Plenio M B 2017 *Rev. Mod. Phys.* **89** 041003
[21] Bera M N, Qureshi T, Siddiqui M A and Pati A K 2015 *Phys. Rev. A* **92** 012118
[22] Bagan E, Bergou J A, Cottrell S S and Hillery M 2016 *Phys. Rev. Lett.* **116** 160406
[23] Yuan Y, Hou Z B, Zhao Y Y, Zhong H S, Xiang G Y, Li C F and Guo G C 2018 *Opt. Express* **26** 4470
[24] Bagan E, Calsamiglia J, Bergou J A and Hillery M 2018 *Phys. Rev. Lett.* **120** 050402
[25] Jaeger G, Shimony A and Vaidman L 1995 *Phys. Rev. A* **51** 54
[26] Jia A A, Huang J H, Zhang T C and Zhu S Y 2014 *Phys. Rev. A* **89** 042103